

OPTIMISATION OF A CRUCIFORM TEST SPECIMEN FOR BI-AXIAL LOADING OF FIBRE REINFORCED MATERIAL SYSTEMS

Smits A.*, Van Hemelrijck D.*, Philippidis T.***, van Wingerde A.M.***, Cardon A.*

* Department of Mechanics of Materials and Constructions (MeMC), Vrije Universiteit Brussel / Free University of Brussels (VUB), Pleinlaan 2, B-1050 Brussels, Belgium

** Department of Mechanical Engineering & Aeronautics, University of Patras, P.O. Box 1401, Patras 265 00, Greece

*** Wind turbine Materials and Constructions, Knowledge Centre WMC, P.O. Box 43, 1770 AA Wieringerwerf, The Netherlands

ABSTRACT

Experimental investigation of fibre reinforced composites was predominantly performed using uni-axially loaded specimens. However, composites are often subjected to complex multi-axial loadings in service and consequently, experimental investigation should consider bi-axial tests. For this reason a bi-axial testing facility for planar cruciform specimens was developed. A valid and useful bi-axial test avoids failure in the uni-axially loaded arms and gives a large region of uniform strain in the bi-axially loaded zone, conditions which are not easily obtained simultaneously. To be able to select a suitable geometry, finite element simulations investigating the influence of various parameters in combination with experiments on different geometries were performed.

1. INTRODUCTION

All too often, mechanical testing of fibre reinforced composites was (and still is) limited to uni-axially loaded specimens. In service, fibre reinforced composites are hardly ever loaded in one direction. Since the material properties are optimized for the primary load, even small secondary loads can lead to failure when they coincide with a weakness in the material. Experimental investigation of these materials should approximate real life behaviour as much as possible. In an attempt to achieve this goal bi-axial tests can be considered [1]. When bi-axial loads are applied, it is usually by superimposing a torsion load on tubular specimens subjected to tension or compression [2, 3]. Real construction components in fibre reinforced composite materials however, are often made in the form of flat or gently curved panels. Moreover, thin-walled tubes are not easy to fabricate and obtaining a perfect alignment and load introduction is not straightforward. Furthermore failure often occurs at the edge due to stress concentrations or local buckling [4, 5]. For this reason a bi-axial testing facility for planar cruciform specimens (Fig. 1) was developed at the Free University of Brussels.

2. PLANAR BI-AXIAL TESTING DEVICE

A bi-axial tension test bench for planar cruciform specimens with a maximum capacity of 100 kN is used. A successful bi-axial loading test satisfies two criteria: a test zone with a uniform bi-axial stress distribution should be obtained, and specimen failure must occur within this bi-axially loaded test zone —not in the uni-axially loaded arms. To fulfil the uniformity requirement, the force P has to be equal and collinear to the P' and the force F equal and collinear to F' (Fig. 2). In addition P & P' has to be perpendicular to F & F' .



Fig. 1. Bi-axial test bench for flat cruciform specimens.

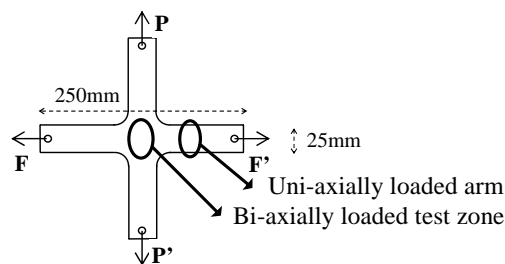


Fig. 2. Cruciform geometry with identification of forces.

In order to maintain the co linearity —i.e., avoid bending moments which cause non-uniform stress distribution in the bi-axially loaded zone— it is desirable that the centre of the specimen does not undergo any displacement. A simple arrangement where two ends of the cruciform specimen are held fixed while the opposite ends are loaded, is unsatisfactory in this respect. Instead, four servo-hydraulic cylinders are used, with a control unit to explicitly keep the forces collinear (Fig. 3). As no cylinders with hydrostatic bearing were used, the test frame is limited to loading in tension. Failure or slip in one arm of the specimen will result in sudden radial forces which could seriously damage the servo-hydraulic cylinders and load cells. To prevent this, hinges were used to connect the specimen with the cylinders and to connect the cylinders to the test frame. Using four hinges for each loading direction results in an unstable situation in compression and consequently only tests in tension can be performed. In an ideal situation the forces are as shown in Fig. 4a and no displacement of the centre point of the specimen is observed. If a displacement occurs (for instance in the Y-direction) an imbalance arises in the forces, as shown in Fig. 4b (a component F_y is added).

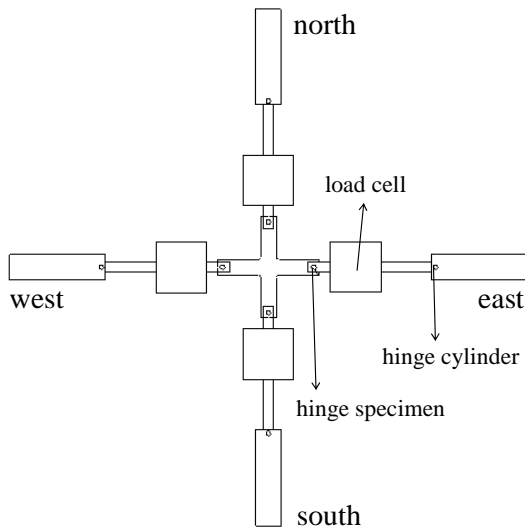


Fig. 3. Schematic illustration of the bi-axial test set-up.

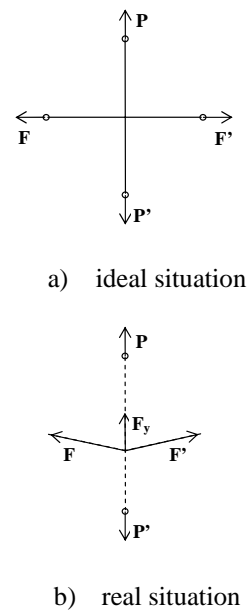


Fig. 4. Forces on the cruciform specimen.

From the force equilibrium in the Y-direction we obtain:

$$P + F_y = P' \quad (1)$$

Due to the displacement, the absolute value of the force $|P|$ is no longer equal to $|P'|$. However as four load cells are used, it is possible to measure this small difference in loads during load controlled tests. In fact, this measured difference is used as a control signal in this direction. The same is done in the perpendicular direction. Thus, active control is used to maintain the co linearity of the applied loads.

3. CRUCIFORM SPECIMEN DESIGN

It has proven extremely difficult to develop a cruciform test specimen that simultaneously fulfils the following conditions: (i) there has to be a uniform strain state in the bi-axially loaded test zone, (ii) failure has to occur in the bi-axially loaded test zone and not in the uni-axially loaded arms, and (iii) the results should be repeatable [3, 5]. To test preliminary

cruciform specimen designs, an initially indicative photo-elastic study was carried out on the isotropic material araldite; then finite element simulations were performed and a selection of final candidate geometries was tested experimentally. To investigate the influence of parameters like (i) the rounding radius at the intersection of the arms, (ii) the thickness of the bi-axial loaded test zone in relation to the thickness of the arms and (iii) the geometry of the bi-axial loaded test zone, finite element simulations were performed in increasing level of complexity. Indicative isotropic simulations were performed to be able to perform a quick evaluation of the influence of certain parameters, and then orthotropic simulations were carried out with the complete lay-up modelled to investigate the influence of the directions of the fibres in the composite material. Afterwards, the numerical results were compared with experimental results obtained on selected cruciform geometries using a digital image correlation technique for full field strain measurement. Strain gauges were also used as a reference.

3.1. Photo-elasticity study and isotropic finite element simulations

Using a circular polariscope, the isochromatic fringes in a cruciform araldite specimen loaded in both vertical and horizontal directions were recorded. The stress distribution was symmetric and also reasonably uniform in the arms and in a certain zone of the bi-axially loaded test area for a specimen without end-tabs (Fig. 5a). Since the aim is to avoid failure in the uni-axially loaded arms, long duralumin end-tabs were glued on them afterwards. For this configuration, a new photo-elasticity study was carried out and the stresses in the bi-axially loaded test zone were symmetric again (Fig. 5b).

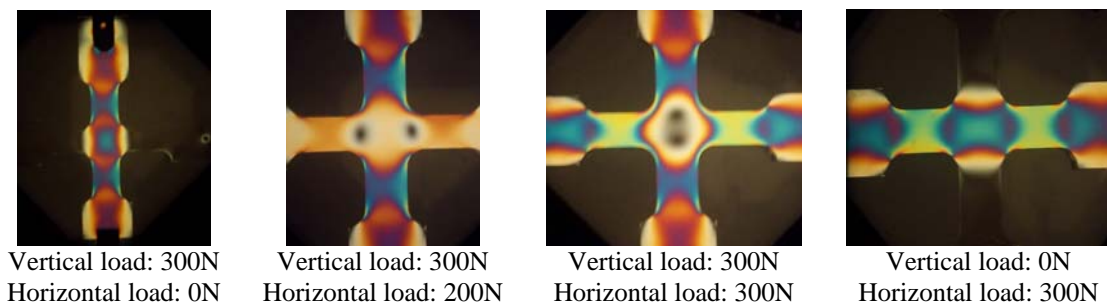


Fig. 5a. Isochromatic fringes in a bi-axially loaded cruciform specimen without end-tabs.

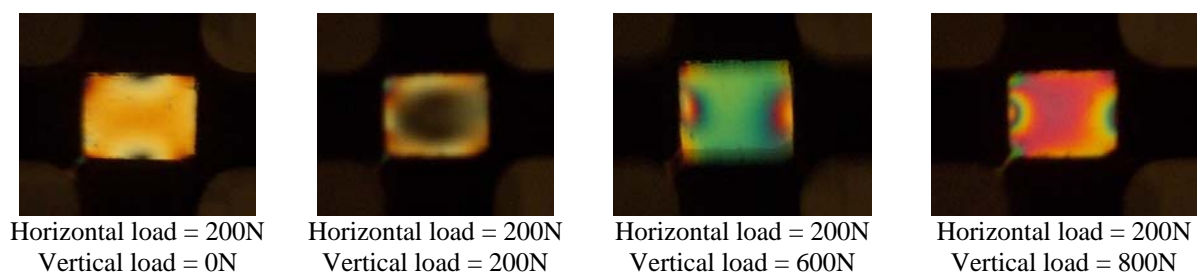


Fig. 5b. Isochromatic fringes in a bi-axially loaded cruciform specimen with end-tabs in duralumin.

Based on these results, isotropic finite element simulations were performed to investigate the influence of various parameters. The material simulated was steel (stiffness modulus $E = 210\text{GPa}$; Poisson's ratio $\nu = 0.3$). The simulations were performed with the commercial software *Ansys inc. 7.1* using element type *shell 99*. This element has six degrees of freedom at each node: three translations and three rotations. It is defined by eight nodes, the average or corner layer thicknesses, the layer material direction angles and the orthotropic material properties. It may be used for layered applications of a structural shell model and allows up to

250 layers. For the isotropic simulations only one layer was used. For the orthotropic simulations that were performed afterwards, the lay-up was modelled with different layers. Strains and stresses are computed at the mid thickness of each layer. Due to symmetry, only one quarter of the geometry of each simulation is shown. The bi-axially loaded test zone was zoomed in, but the finite element calculation was performed with much longer arms. All geometries were loaded equally in both directions with a force $F_x=F_y=20.5\text{kN}$. Fig. 6 shows the finite element results of the first principal strains. The geometries have a thickness of 6.57mm (zone [2] on Fig. 6). Where material was milled away in the thickness direction at the middle zone as in geometries B, C and D, the remaining thickness is 3.59mm (zone [3]).

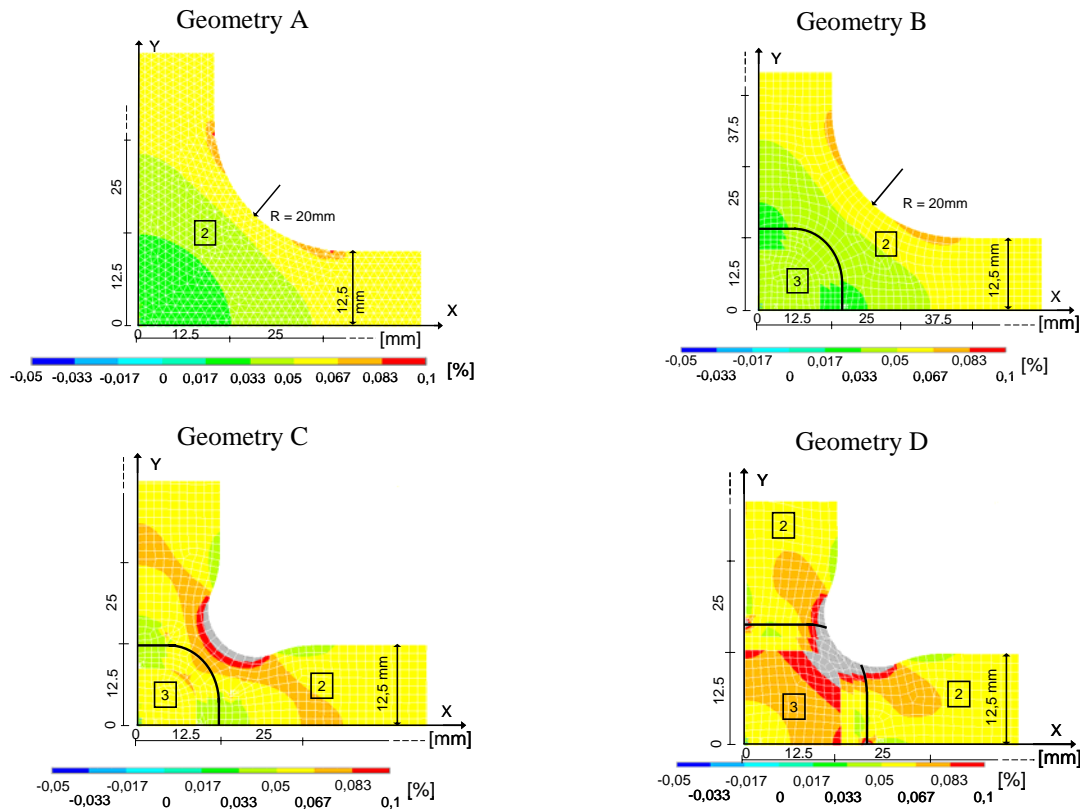


Fig. 6. Isotropic finite element results for three cruciform specimens. First principal strains are shown.

Geometry A shows the first principal strain results for a geometry of constant thickness with a radius $R = 20\text{mm}$ between two perpendicular arms. The highest strains occur in the uni-axially loaded arms, so the failure mode for this kind of geometry is not really representative of the bi-axial loading condition. In order to increase the strains —and the likelihood of failure— in the bi-axially loaded zone, a reduction of the thickness in the bi-axially loaded test zone was applied in geometry B. Strains increased in the zone of interest but not sufficiently. The uni-axially loaded arms maintain the highest strain results. In geometry C a combination of a thickness reduction and changing the rounding radius at the intersection of two perpendicular arms from outside the geometry towards inside was studied. The strain results are improved, but highest strains occur now at the rounding radius and still not at the centre of the specimen. In geometry D a larger area of reduced thickness was used, resulting in higher strains in the bi-axially loaded test zone. None of the studied geometries were completely satisfying, but adding long end-tabs at the uni-axially loaded specimens would probably lead to better results. These end-tabs should probably pass the start of the rounding radius.

3.2. Orthotropic finite element simulations including lay-up of the composite material

Fig. 8 shows the finite element results of the first and second principal strains for three geometries A, B and C modelled as glass fibre reinforced epoxy with a $[(+45^\circ -45^\circ 0^\circ)_4(+45^\circ -45^\circ)]$ -lay-up (zone 2 on Fig. 8 with lay-up 2 on Fig. 7). This material with this specific lay-up is often used for wind turbine rotor blades, as they are globally submitted to bending combined with torsion. The $(\pm 45^\circ)$ -layers serve to carry torsion and the 0° -layers to carry bending. The load ratio between the x- and y-directions was chosen equal to the strength ratio of both arms i.e. 3.85/1 (Table 1). The $(\pm 45^\circ)$ -layers have a thickness of 0.611mm; the 0° -layers of 0.88mm. This gives a total thickness of 6.57mm for zone 2 and 3.59mm for zone 3. The end-tabs are 2.5mm in thickness each.

Table 1. Uni-axial properties of the tested glass fibre reinforced epoxy composite.

property	dimensions	average	stdev
longitudinal stiffness modulus, E_x	(GPa)	28,70	1,01
transverse stiffness modulus, E_y	(GPa)	15,15	0,78
Poisson's ratio, ν_{xy}	(-)	0,47	0,05
Poisson's ratio, ν_{yx}	(-)	0,28	0,06
longitudinal tensile strength, X	(MPa)	553,8	18,7
longitudinal tensile failure strain, ϵ_x	(%)	2,45	0,09
transverse tensile strength, Y	(MPa)	143,9	3,0
transverse tensile failure strain, ϵ_y	(%)	2,90	0,17

End-tabs were glued on the arms of all the specimens (zone 1). In the middle of geometries B and C a layer of $(0^\circ +45^\circ -45^\circ)$ was milled away at each side of the specimen (zone 3). The applied forces simulated were $F_x/F_y = 46.2\text{kN}/12\text{kN}$.

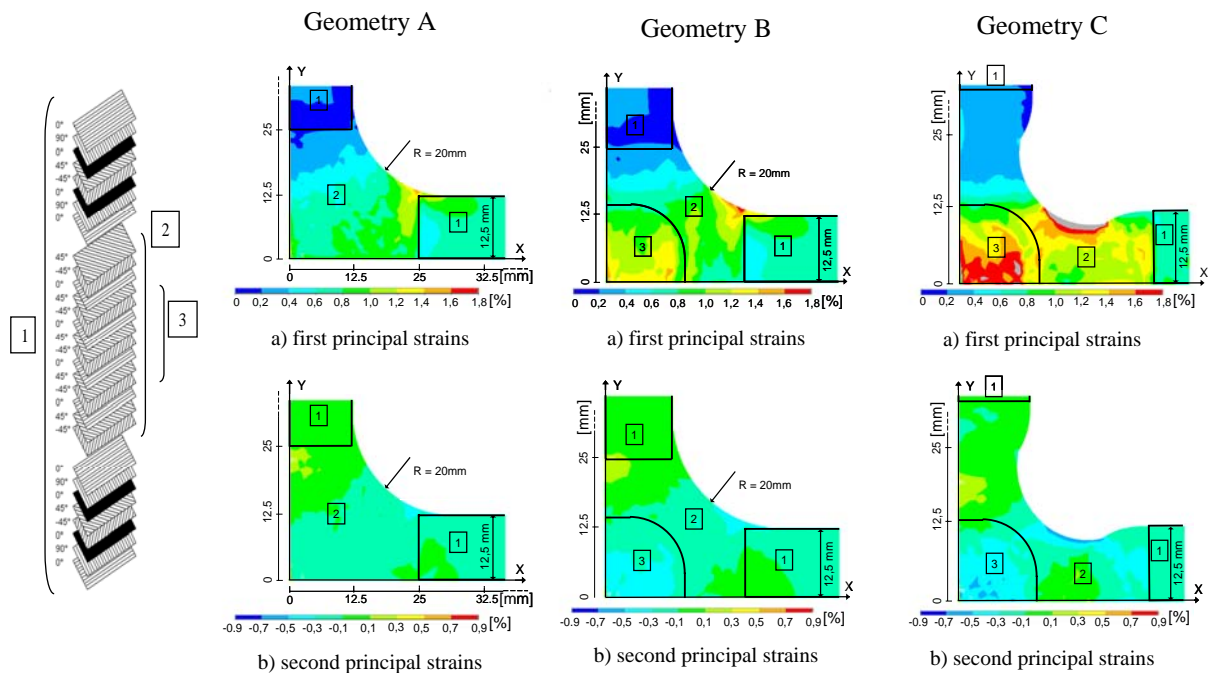


Fig. 7. Lay-up.

Fig. 8. Orthotropic finite element results for three cruciform specimens. First and second principal strains are shown.

For geometry A, the first principal strains in the x-direction just beyond the end-tabs are higher than in the end-tabs, but are lower in the neighbourhood of the centre of the specimen. This is due to the enlargement of the area taking the load in this region. Consequently, failure of the specimen will occur close to the end-tabs. In order to increase the strains and the likelihood of failure in the bi-axially loaded zone, a reduction of the thickness and/or changing the rounding radius at the intersection of two perpendicular arms is necessary. In geometry B the first suggestion is shown. The strain results are improved; for this kind of geometry failure can occur at the middle of the specimen. If we use a combination of both suggestions, as shown in geometry C, even higher strains are obtained in the bi-axial loaded zone.

3.3. Experiments on cruciform specimens

a) Strain gauges

The experimental results for the three tested geometries A, B and C are shown in Table 2. Each value is an average of at least three experiments. Strain measurements were obtained in x- and y- direction by using rosette strain gauges of 6mm length glued in the centre of each specimen. The failure loads and failure strains were measured in both perpendicular directions. With these strain gauges only one average value of the strains is obtained for the two directions. No information regarding the uniformity of the strains in the bi-axially loaded test zone is captured. For that purpose full field strain measurement techniques are needed, as elaborated in the next paragraph. Failure stresses could not be calculated from the failure forces, since the load-bearing area is ill-defined with a cruciform geometry. Therefore, the failure stresses were calculated from the experimentally obtained failure strains using the stiffness moduli and Poisson's ratios measured on uni-axially loaded specimens (Table 1). The formulas giving the strains ε_x in the x-direction and ε_y in the y-direction in function of the occurring stresses σ_x and σ_y are:

$$\varepsilon_x = \sigma_x/E_x - \nu_{xy}\sigma_y/E_y \qquad \varepsilon_y = -\nu_{yx}\sigma_x/E_x + \sigma_y/E_y \qquad (2)$$

Conversely, stresses can be calculated from the measured strains:

$$\sigma_y = (\varepsilon_y + \nu_{yx}\varepsilon_x) E_y / (1 - \nu_{yx}\nu_{xy}) \qquad (3)$$

$$\sigma_x = (\varepsilon_x + \nu_{xy}\sigma_y/E_y) E_x = (\varepsilon_x + \nu_{xy}(\varepsilon_y + \nu_{yx}\varepsilon_x) / (1 - \nu_{yx}\nu_{xy})) E_x$$

The results of the obtained failure loads, failure strains and calculated failure stresses are shown in Table 2.

Table 2. Experimental results of three cruciform specimens.

	[kN]		[%]		[MPa]	
	F_x	F_y	ε_x	ε_y	σ_x	σ_y
geometry A	63,2	16,5	1,35	-0,56	395	14
geometry B	60,5	15,8	1,52	-0,66	442	13
geometry C	47,9	12,4	1,68	-0,47	516	56

The highest failure strains are obtained for geometry C, indicating this geometry is the most promising one. For geometry A, failure of the specimen didn't occur in the bi-axial loaded test zone, whereas in geometries B and C it did. Pictures recorded immediately prior to (upper frame) and during failure (lower frame) are shown in Fig. 9 for each of the three geometries.

These results confirm the results of the finite element simulations. The high values for the experimentally obtained failure strains indicate that the strain concentrations at the rounding between the two perpendicular arms in geometry C —seen in the finite element simulations— do not cause early failure of the specimen.

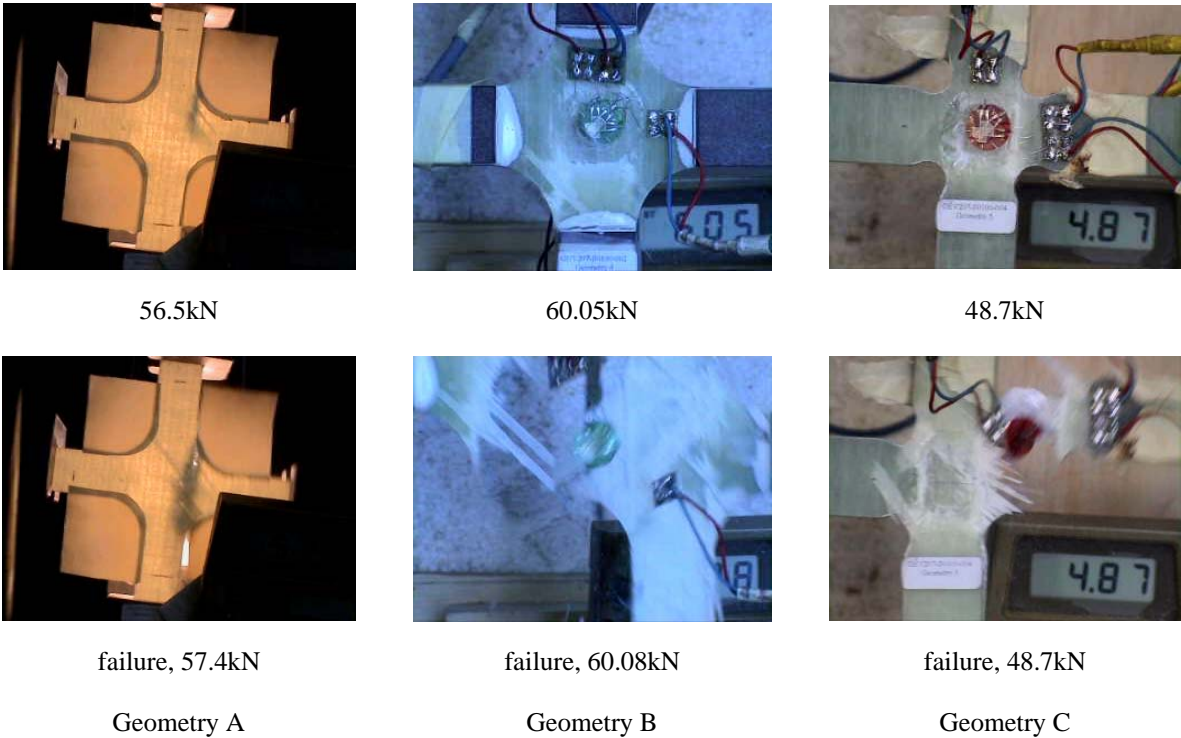


Fig. 9. Failure of cruciform specimens.

For all geometries, failure starts at the rounding radius between the two arms —not from the middle of the specimen— but for geometries B and C the whole bi-axially loaded test zone is damaged afterwards. Also the high measured strains in the middle of the specimen indicate that the starting of the failure at the rounding radius does not cause early failure of the specimen.

b) The digital image correlation technique

Digital image correlation is a full field measurement technique that detects deformations using image processing. Once the deformations of a speckle pattern applied to the specimen have been measured, the strain distribution in the material can be calculated. This allows the uniformity of strains in a certain zone to be judged. The fundamental principle of this technique is based on the correspondence, for a large number of distinguishable small areas —known as macro image facets— between the distribution of grey scale values in the undeformed state and the distribution of grey scale values of the same area in the deformed state. The only limitation is that each facet must contain grey value gradients in both coordinate directions. This technique can allocate coordinates to every pixel in digital images. By tracking the facets in each successive image with sub-pixel accuracy, relative displacements are obtained and the resulting strains can be derived [6]. In Fig. 10 the strain results obtained with the digital image correlation technique are compared with the finite element simulation results for geometry B, i.e., with a milled surface in the middle of the specimen and with a rounding radius of 20mm. The pictures were taken immediately prior to failure of the specimen at a load of $F_x/F_y=61.6\text{kN}/16\text{kN}$.

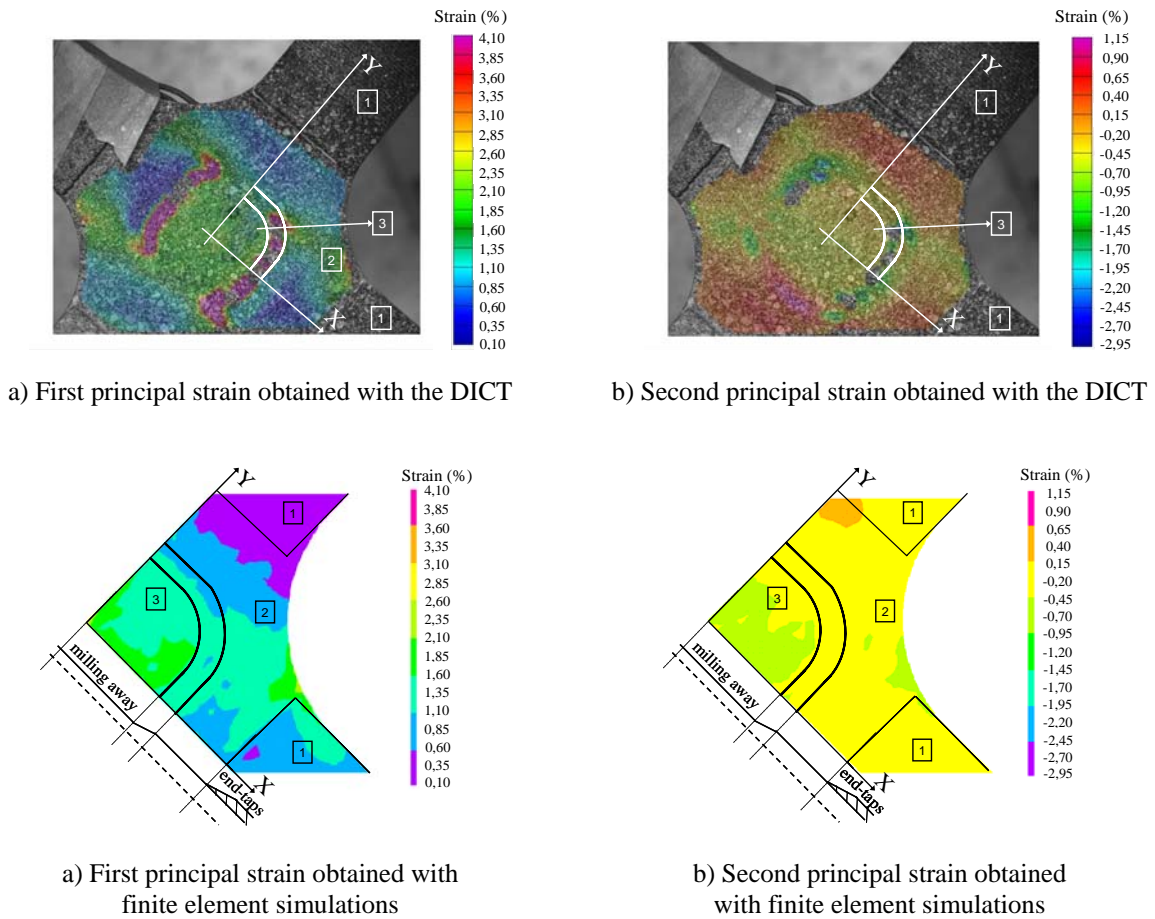


Fig. 10. Comparison between results of the digital image correlation technique and finite element simulations.

The results of the digital image correlation and the finite element simulations are substantially in agreement, both for the first and second principal strains. Only in the transition zone between the full thickness and the milled area, high strains are observed with the digital image correlation technique but not in the finite element simulations. This may be due to the fact that only one camera was used, able to detect only in plane displacements on flat areas accurately.

4. CONCLUSIONS

The combination of finite element simulations and experiments performed on three different geometries of cruciform specimens, led to the selection of a suitable geometry for bi-axial testing of composite materials. This geometry has a reduced thickness in the central region of the specimen, in combination with a rounding radius between two arms inside the material. These features cause failure to occur in the bi-axially loaded test zone, rather than in the uni-axially loaded arms. The digital image correlation technique used for full field strain measurements offers significant advantages over conventional techniques such as strain gauges. The high data point density of the results lead to a better understanding of the behaviour of composites under bi-axial loads. The strain values obtained with the digital image correlation technique are comparable with those measured using strain gauges at the centres of the specimens and with those calculated in the finite element simulations. The strain distribution throughout the bi-axially loaded test zone can be considered as quite uniform.

ACKNOWLEDGEMENTS

This research is partially funded by the European Commission in the framework of the specific research and technology development programme Energy, Environment and Sustainable Development with contract number ENK6-CT-2001-00552. The authors also express their gratitude to Hans Tommerup Knudsen from LM-Glassfiber in Denmark for his effort in producing the cruciform specimens.

References:

1. **Soden, P. D., Hinton, M. J., Kaddour A. S.**, "Predicting failure in composite laminates: the background to the exercise", *Composites Science and Technology*, **58/7** (1998), 1001-1010.
2. **Soden, P. D., Hinton, M. J., Kaddour, A. S.**, "A comparison of the predictive capabilities of current failure theories for composite laminates", *Composites Science and Technology*, **58/7** (1998), 1225-1254.
3. **Welsh, J. S. and Adams, D. F.**, "An experimental investigation of the biaxial strength of IM6/3501-6 carbon/epoxy cross-ply laminates using cruciform specimens", *Composites Part A: Applied Science and Manufacturing*, **33/6** (2002), 829-839.
4. **Smith, E. W. and Pascoe, K. J.**, "Biaxial fatigue of a glass-fibre reinforced composite. Part 2: Failure criteria for fatigue and fracture", *Mechanical Engineering Publications*, London, Appendix 1.
5. **Dawicke, D. S. and Pollock, W. D.**, "Biaxial testing of 2219-T87 aluminum alloy using cruciform specimens", *NASA Contractor Report 4782*, (1997).
6. **Tyson J., Schmidt T., Galanulis K.**, "Advanced photogrammetry for robust deformation and strain measurement", *accepted for proceedings at SEM 2002 Annual conference*, Milwaukee, WI